RSC Advances

PAPER

View Article Online
View Journal | View Issue

Cite this: *RSC Adv.*, 2023, **13**, 3033

High-efficiency catalyst $CuSO_4$/SBA-15 toward butylated hydroxytoluene synthesis in a heterogeneous system†

Yi-Jie Wang, Yu-Fen Bao, Xiao-Jie Lu, Jia-Qi Dong and Ding-Hua Liu*

Received 8th December 2022
Accepted 6th January 2023

DOI: 10.1039/d2ra07835j

rsc.li/rsc-advances

An SBA-15 loaded $CuSO_4$ catalyst was designed and prepared for the highly selective production of 2,6-di-*tert*-butyl-*p*-cresol (BHT) from *p*-cresol and isobutylene. The acidity of solid acid catalysts was altered by varying the loading amount of $CuSO_4$. Among them, 10% $CuSO_4$/SBA-15 exhibited the greatest catalytic performance in the alkylation reaction with a BHT yield of 85.5%. After four cycles, the yield of BHT exceeded 70%. Overall, the catalyst has excellent catalytic performance and can be utilized as a catalyst for efficient BHT production.

1. Introduction

2,6-Di-*tert*-butyl-*p*-cresol (butylated hydroxytoluene, BHT) is an important phenolic antioxidant widely utilized in rubber, petroleum products, food, essential oils, cosmetics, *etc.*[1–5] Nowadays, three methods have been developed to synthesize BHT, including the *p*-cresol, phenol, and mixed cresol techniques. Among these, the synthesis with *p*-cresol as a raw material has a high degree of economic viability and is frequently employed in industrial production.[6–8] The mechanism of the reaction is depicted in Fig. 1. First, isobutylene forms a *tert*-butyl cation in the presence of an acid catalyst. The *tert*-butyl cation then performs an electrophilic addition reaction with *p*-cresol to generate mono-*tert*-butyl *p*-cresol. Mono-*tert*-butyl-*p*-cresol finally interacts with a *tert*-butyl cation to create BHT. Concurrently, *tert*-butyl cations and isobutylene polymerize to create polymers.[9] This side effect can significantly reduce the yield of BHT.

Until now, most of the catalysts used in BHT synthesis are sulfuric acid and *p*-toluene sulfonic acid.[10–13] Although the use of this type of catalyst provides the benefits of high catalytic activity, it can cause problems such as equipment corrosion, difficult separation of catalysts, and the generation of large amounts of industrial wastewater. This not only raises manufacturing costs, but the discharge of huge quantities of industrial wastewater can also result in environmental pollution.[14,15] In the last few years, the utilization of new acid catalysts, such as sulfated ZrO_2,[16,17] WO_3/ZrO_2,[18] 12-phosphotungstic acid/TiO_2,[19] and 12-phosphotungstic acid/ZrO_2,[20] has been paid great attention. Despite the ease of separation and high activity of these catalysts, the presence of a large number of micropores leads to the rapid accumulation of polymers within the pore channels, resulting in the deactivation of catalysts. SBA-15 is a catalyst carrier with applications in catalysis, separation, biology, and nanomaterials.[21–30] SBA-15 possesses highly ordered mesoporous structure, high specific surface area, adjustable pore size, high thermal and hydrothermal stability.[31,32] Therefore, the introduction of SBA-15 mesopores will help to improve the stability of the catalysts.

Since an excessively strong acid may promote the polymerization of isobutene, the selection of acid sites with appropriate strength is necessary to achieve catalyst recyclability. Copper sulphate is a moderate Lewis acid salt that is commonly applied in solid acid catalysts such as $CuSO_4/TiO_2$,[33,34] $CuSO_4/SiO_2$,[35,36] $CuSO_4$/HZSM-5,[37] $CuSO_4/Al_2O_3$,[38] *etc.* These catalysts are mostly utilized for cycloaddition, esterification, and aromatization reactions, but their application in alkylation reactions has not been studied.

In this work, different amounts of copper sulfate were loaded on SBA-15 to produce catalysts for the alkylation reaction of *p*-cresol and isobutene. The effects of reaction temperature, catalyst loading, and reaction time on the yield of BHT were studied, and the recyclability of the catalyst was explored.

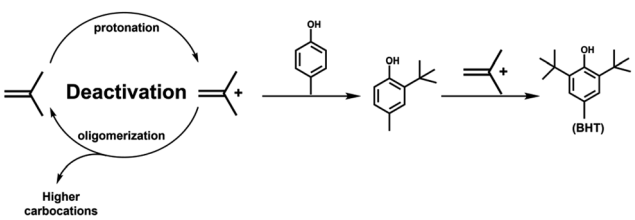

Fig. 1 Catalytic reaction mechanism of *p*-cresol with isobutene.

State Key Laboratory of Materials-Oriented Chemical Engineering, College of Chemical Engineering, Nanjing Tech University, Nanjing 210009, China. E-mail: ncldh@njtech.edu.cn

† Electronic supplementary information (ESI) available. See DOI: https://doi.org/10.1039/d2ra07835j

2. Experimental

2.1 Materials

P-cresol (99%), anhydrous copper sulfate (99%) and ethanol (99%) were purchased from Aladdin Industrial Corporation. Hydrochloric acid (HCl, 37%), sulfuric acid (98%) and tetraethyl orthosilicate (TEOS, 99%) were purchased from Sinopharm Chemical Reagent Corporation. Pluronic@P-123 (PEG_{20}-PPG_{70}-PEG_{20}, $M_n \sim 5800$) was purchased from Sigma-Aldrich. Isobutylene (99%) was purchased from Nanjing Special Gas Corporation. All reagents were used without further purification.

2.2 Preparation of $CuSO_4$/SBA-15 materials

$CuSO_4$/SBA-15 was prepared with the procedure shown in Fig. 2. The mesoporous silica SBA-15 was synthesized according to the approach reported by Zhao *et al.*[39] In a typical synthesis method, 3 g of the template agent Pluronic@P-123 was dissolved in a mixture of 90 g of 2 M HCl solution and 22.5 g of deionized water, and stirred at a constant temperature of 40 °C for 2 h. Then 6.38 g of TEOS was slowly added and stirred for 24 h. After ageing, the sample was poured out, filtered, and air-dried at 60 °C to obtain SBA-15 with a template agent, noted as AS. Then AS was calcined at 550 °C in an air atmosphere for 5 h to eliminate the template agent, noted as CS.

A certain amount of $CuSO_4$ was dissolved in 40 mL of dilute sulfuric acid solution with a mass fraction of 5%, and then 5.0 g of SBA-15 was added to the $CuSO_4$ solution. After 30 min of sonication, the sample was left to stand for 24 h, dried in an oven at 120 °C, and then calcined at 250 °C for 5 h under a nitrogen atmosphere to obtain the catalyst. The catalysts were denoted as *x*$CuSO_4$/SBA-15, where *x* represents the weight proportion of $CuSO_4$ in the catalyst.

2.3 Catalyst activity study

The reaction of *p*-cresol with isobutylene was carried out in a three-necked flask. In a typical reaction, 3.0 g of catalyst and 30 g of *p*-cresol were added to a three-necked flask. The three-necked flask was placed in an oil bath with magnetic stirring (550 rpm) and preheated to the specified temperature. Subsequently, isobutylene gas was introduced and the flow rate was controlled at 20 mL min^{-1} to allow sufficient reaction. For the sampling, 0.5 mL of the upper reaction solution was dissolved in 1.5 mL of ethanol and analyzed by gas chromatography. The yield of BHT was defined as follows:

$$\text{Yield of BHT (\%)} = \text{actual BHT weight/theoretical BHT weight} \times 100\%$$

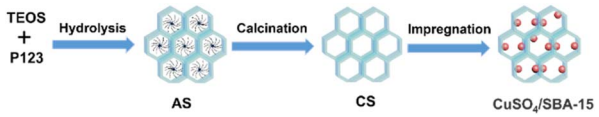

Fig. 2 Preparation of $CuSO_4$/SBA-15 catalyst.

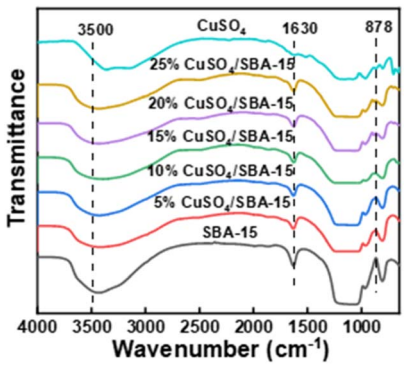

Fig. 3 FT-IR spectra of $CuSO_4$/SBA-15.

3. Results and discussion

3.1 Catalyst characterization

Fig. 3 represents the FT-IR spectra of catalysts with various $CuSO_4$ loadings. All samples exhibited broad bands centered at 1630 cm^{-1} and 3500 cm^{-1}, corresponding to stretching vibrations of different hydroxyl groups, such as surface Si–OH groups, bridged hydroxyl groups, and H_2O molecules. The absorption peaks at 800 cm^{-1}, 989 cm^{-1} and 1300 cm^{-1} were attributed to various bending, asymmetric, and symmetric vibrations of the Si–O–Si bridging atoms, which are characteristic bands of SBA-15.[22] The absorption peak at 878 cm^{-1} corresponded to the stretching vibration peak of the S=O bond in $CuSO_4$, and its intensity increased significantly with the $CuSO_4$ loading, indicating that the sulphate group was successfully introduced into the pore channel. The intensity of the broad band around 3500 cm^{-1} increased with $CuSO_4$ loading, which also confirmed the coverage of the Si surface by hydrophilic $CuSO_4$.

The low-angle XRD patterns of SBA-15 and $CuSO_4$/SBA-15 catalysts are displayed in Fig. 4(a) and S1.† The characteristic peaks with 2θ of *ca.* 0.5°, 0.7°, and 0.9° for SBA-15 were also present in the spectra for $CuSO_4$/SBA-15, which were related to (100), (110), and (200) crystal planes. Consequently, the unique mesoporous feature of SBA-15 was preserved after the modification with $CuSO_4$. The wide-angle XRD of $CuSO_4$/SBA-15 catalysts displayed in Fig. 4(b) revealed that the diffraction peaks corresponding to the crystalline planes (021), (030), (111), and

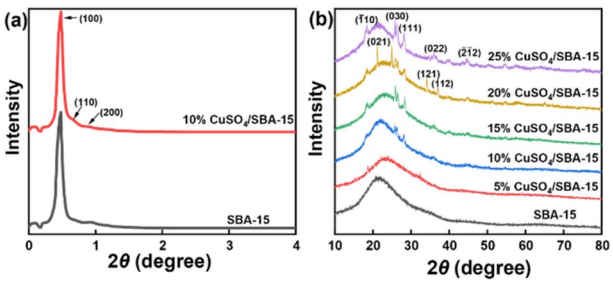

Fig. 4 (a) Low angle XRD pattern (b) wide angle XRD pattern of $CuSO_4$/SBA-15.

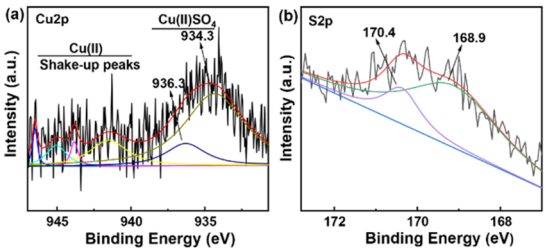

Fig. 5 XPS spectra of (a) Cu 2p and (b) S 2p for 10% $CuSO_4$/SBA-15.

(121) of $CuSO_4$ appeared on the spectra, and the intensity of the peak increased gradually with the increase in $CuSO_4$ loading, indicating that $CuSO_4$ was effectively complexed with SBA-15.

The XPS spectra of 10% $CuSO_4$/SBA-15 are presented in Fig. 5. It can be seen that the Cu species supported on SBA-15 is divalent, and the Cu 2p spectrum can be divided into two peaks at 934.3 eV and 936.3 eV, which are characteristic peaks of $CuSO_4$.[33,40] Meanwhile, the presence of $CuSO_4$ leads to the shake-up peaks.[41] This demonstrated that $CuSO_4$ could still be effectively retained on SBA-15 after the catalyst was calcined at a high temperature and that the catalyst held high thermal stability. Besides, the S 2p spectrum could be acquired with two peaks at 168.9 eV and 170.4 eV, corresponding to the S of $CuSO_4$, which confirmed the successful preparation of $CuSO_4$/SBA-15 catalyst.

Fig. 6 illustrates the TG curves of SBA-15 and $CuSO_4$/SBA-15 (5–25%). As can be seen, the quality of the SBA-15 carrier did not decline appreciably when heated to 900 °C, indicating its great thermal stability. $CuSO_4$/SBA-15 (5–25%) underwent three stages of mass loss. The first loss of 8.5% between 40 °C and 102 °C was caused by physical absorption of water. The second stage was a loss of 7.04% between 102 °C and 620 °C from the weight loss of copper sulfate crystalline water and structural water. The catalyst degraded dramatically between 620 °C and 900 °C due to the breakdown of $CuSO_4$ into CuO and SO_3. Overall, the TG results confirmed the high thermal stability of the $CuSO_4$/SBA-15 catalyst. Consequently, the $CuSO_4$/SBA-15 catalyst has the potential to exhibit good catalytic activity in the Foucault alkylation reaction.

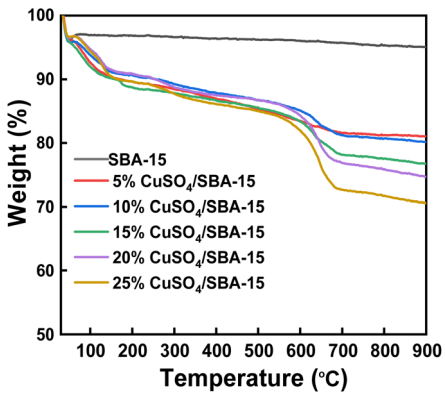

Fig. 6 TG analysis of $CuSO_4$/SBA-15.

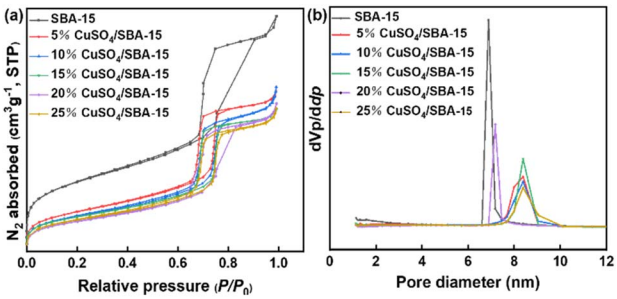

Fig. 7 (a) N_2 adsorption–desorption isotherms of $CuSO_4$/SBA-15 and (b) pore size distribution of $CuSO_4$/SBA-15.

Table 1 Physicochemical properties of $CuSO_4$/SBA-15

Sample name	BET surface area ($m^2\ g^{-1}$)	Pore volume ($cm^3\ g^{-1}$)	Average pore size (nm)
SBA-15	832	1.09	5.22
5%	521	0.81	6.24
10%	474	0.82	6.95
15%	453	0.72	6.34
20%	422	0.75	7.06
25%	427	0.72	6.73

Fig. 7 depicts the N_2 adsorption–desorption isotherms and corresponding pore size distribution curves of the catalysts with different $CuSO_4$ loadings. From Fig. 7(a), all catalysts exhibited type IV isotherms. SBA-15 carrier possessed a large pore volume and a high specific surface area. Meanwhile, the weight proportion of $CuSO_4$ in the sample had a great effect on the BET specific surface area, total pore volume, and average pore size (Table 1). With the weight proportion of $CuSO_4$ increased from 5% to 25%, the BET specific surface area of SBA-15 decreased from 832 $m^2\ g^{-1}$ to 427 $m^2\ g^{-1}$, correspondingly, and in the meanwhile the pore volume decreased gradually. After loading with $CuSO_4$, the average pore size of the samples tended to increased. This was due to the blockage of microporous pore channels with increasing loading and the collapse of some pores in SBA-15 after $CuSO_4$ treatment. Fig. 7(b) depicts the pore size distribution of the samples, and it can be seen that $CuSO_4$/SBA-15 had a channel size between 6–10 nm, confirming that the mesoporous structure of SBA-15 was preserved after immobilization of $CuSO_4$. Because of its high specific surface area and large pore size, $CuSO_4$/SBA-15 is expected to demonstrate good catalytic activity in the alkylation reaction.

Surface morphology and distribution of Cu and S in the catalysts were examined by SEM (Fig. S2†) and EDS trace element mapping (Fig. 8). From Fig. S2,† the SBA-15 carrier retained its wheat shape and smooth surface after modification with $CuSO_4$. From the EDS trace element profiles in Fig. 8, it can be seen that Cu and S elements were uniformly distributed in the SBA-15 material, and the content of Cu and S elements increased significantly with the increase in loading. In addition, the pore structures of the SBA-15 carrier and copper sulfate catalyst were examined by TEM. From the TEM image (Fig. 9), it

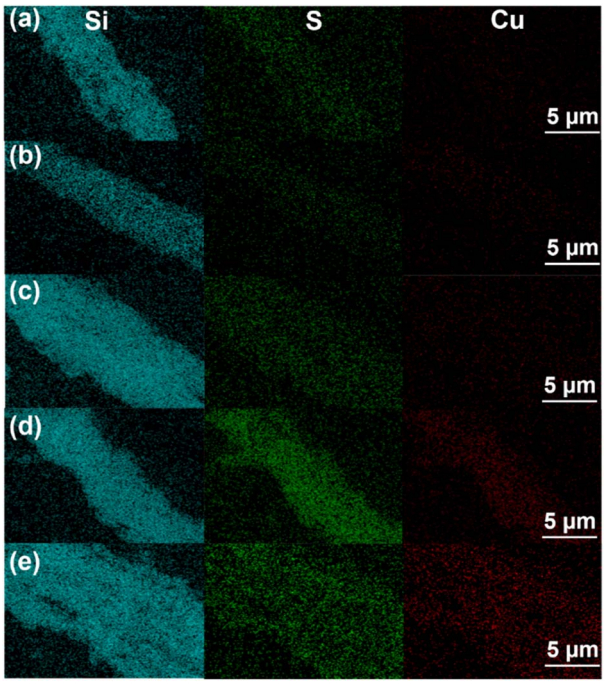

Fig. 8 SEM-EDS microelement mapping of (a) 5% $CuSO_4$/SBA-15, (b) 10% $CuSO_4$/SBA-15, (c) 15% $CuSO_4$/SBA-15, (d) 20% $CuSO_4$/SBA-15 and (e) 25% $CuSO_4$/SBA-15.

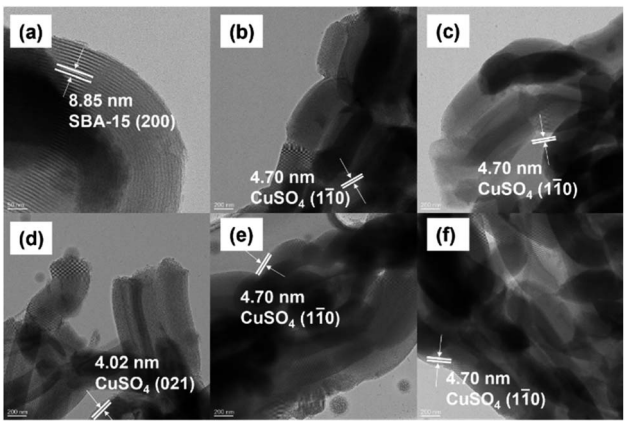

Fig. 9 TEM images of (a) SBA-15, (b) 5% $CuSO_4$/SBA-15, (c) 10% $CuSO_4$/SBA-15, (d) 15% $CuSO_4$/SBA-15, (e) 20% $CuSO_4$/SBA-15 and (f) 25% $CuSO_4$/SBA-15.

can be clearly seen that SBA-15 was not affected by the deposition of $CuSO_4$ particles and still maintained the regular pore structure of SBA-15, which confirmed the high stability of SBA-15. SBA-15 has a lattice fringe with an interplanar spacing of 8.85 nm, which was consistent with the (200) lattice plane. Each catalyst displayed lattice stripes with lattice spacings of 4.02 nm and 4.70 nm, corresponding to the (1$\bar{1}$0) and (021) lattice planes of $CuSO_4$. Therefore, $CuSO_4$ was successfully loaded onto SBA-15, consistent with the XRD data presented before.

3.2 Catalyst performance evaluation

3.2.1 Influence of reaction conditions. The effect of reaction time was investigated at 80 °C using 10% $CuSO_4$/SBA-15 catalyst, and the results are shown in Fig. 10(a). In the initial stage, the BHT yield increased rapidly, reaching 80.21% after 2.5 h of reaction. However, when the reaction time increased to 4.5 h, the BHT yield remained essentially unchanged, demonstrating that equilibrium could be reached within 4.5 h and the catalyst had a high catalytic activity. Fig. 10(b) demonstrated that the change in temperature had a significant influence on the reaction. As the reaction temperature increased, the production of BHT increased initially and then declined. An increase in temperature was beneficial for the isobutene synthesis reaction, but it also increased the polymerization of isobutene, resulting in a large volume of high-polymer isobutene. Consequently, the optimal temperature for this reaction was 80 °C. The catalytic activity of the catalysts with different $CuSO_4$ loadings are presented in Fig. 10(c). When $CuSO_4$ was added to SBA-15, all catalysts held high BHT yields. Among them, 10%$CuSO_4$/SBA-15 has the highest product yield (85.5%).

Furthermore, different catalysts were utilised to catalyse this reaction. The results are displayed in Table S5, S6, and S10.† Firstly, isobutene cannot react with *p*-cresol without a catalyst, so no product was generated. When using $CuSO_4$ as catalyst, the catalytic activity was lower. However, when $CuSO_4$ was introduced to SBA-15, the catalytic activity was greatly enhanced. Due to the high acidity of the sulfated SBA-15 catalyst, its catalytic activity was not excellent, resulting in the production of a considerable number of by-products (Table S5†). In addition, different mesoporous materials were utilised as supports for

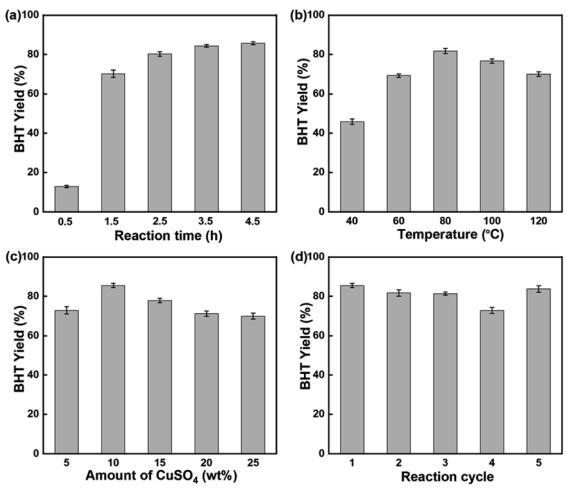

Fig. 10 (a) Effect of reaction time on the yield of BHT. Reaction conditions: reaction temperature = 80 °C, reaction catalyst was 10% $CuSO_4$/SBA-15. (b) Effect of reaction temperature on the yield of BHT. Reaction conditions: reaction time = 4.5 h reaction catalyst was 10% $CuSO_4$/SBA-15. (c) Effect of loading on the yield of BHT. Reaction conditions: reaction time = 4.5 h, reaction temperature = 80 °C. (d) Cycling stability of the catalyst. Reaction conditions: reaction time = 4.5 h, reaction temperature = 80 °C, reaction catalyst was 10% $CuSO_4$/SBA-15.

$CuSO_4$ catalysts, and it can be seen that, SBA-15 with a high specific surface area had higher catalytic activity (Table S6†). Finally, different Lewis acid salts were used as the active sites for the catalysts. $CuSO_4$/SBA-15 exhibited excellent catalytic performance (Table S10†). In summary, the catalytic activity of the catalyst had a high correlation with its specific surface area and acidity. Due to the low specific surface area of $CuSO_4$, it is difficult for the reactants to contact with the catalyst, resulting in its low catalytic activity. When $CuSO_4$ was supported on SBA-15, $CuSO_4$ was highly dispersed in SBA-15, which increased the specific surface area of $CuSO_4$ catalyst, so that $CuSO_4$/SBA-15 catalyst can well catalyse the Friedel–Crafts alkylation reaction of *p*-cresol and isobutylene. Further, the moderate acidity of $CuSO_4$ reduced the generation of polymers and improved catalytic activity of the catalyst.

3.2.2 Recoverability of $CuSO_4$/SBA-15 catalyst. The impact of reaction cycle on BHT yield of $CuSO_4$/SBA-15 was evaluated and is displayed in Fig. 10(d). Although the BHT yield decreased after four cycles, the catalyst still retained a high level of catalytic activity. The decrease in reactivity with cycle was closely related to loss of acid sites by their leaching from SBA-15 and pore blocking of polymers from the polymerization of isobutylene in the reaction. After 4 repetitions, the catalyst was washed with dichloromethane and vacuum-dried at 80 °C, and it recovered its original catalytic activity. However, when other catalysts were utilised to catalyse this reaction, the stability of the catalyst was not ideal (Tables S8, S9, S11 and S12†). Consequently, the $CuSO_4$/SBA-15 catalyst exhibited good catalytic activity and reusability.

4. Conclusions

An efficient and reusable $CuSO_4$/SBA-15 catalyst was prepared by a simple impregnation method by loading Lewis acid salts into the ordered mesoporous material SBA-15. According to the performance evaluation results, 10% $CuSO_4$/SBA-15 possessed great catalytic activity in the alkylation reaction of *p*-cresol. The high catalytic performance of 10% $CuSO_4$/SBA-15 (85.5% BHT yield) was attributed to the Lewis acidity of $CuSO_4$ and the high specific surface area of SBA-15. $CuSO_4$/SBA-15 can be utilized effectively for the alkylation of *p*-cresol and isobutylene due to its low cost, ease of preparation, high catalytic activity, and high stability.

Author contributions

Yi-Jie Wang: investigation, data curation, writing – original draft, writing – review & editing-supporting. Yu-Fen Bao: investigation, writing – review & editing-supporting. Jia-Qi Dong: investigation. Ding-Hua Liu: funding acquisition, project administration, supervision, writing – review & editing.

Conflicts of interest

The authors declare that they have no conflict of interest.

Acknowledgements

This work was supported by the Project of Priority Academic Program Development of Jiangsu Higher Education Institutions and the Six Talent Peaks Project in Jiangsu Province (2014-XCL-016).

References

1 S. K. Mishra, P. D. Belur and R. Iyyaswami, *Int. J. Food Sci. Technol.*, 2021, **56**, 1–12.
2 X. Q. Xu, A. M. Liu, S. Y. Hu, I. Ares, M. R. Martinez-Larranaga, X. Wang, M. Martinez, A. Anadon and M. A. Martinez, *Food Chem.*, 2021, **353**, 129488.
3 W. A. Yehye, N. A. Rahman, A. Ariffin, S. B. A. Hamid, A. A. Alhadi, F. A. Kadir and M. Yaeghoobi, *Eur. J. Med. Chem.*, 2015, **101**, 295–312.
4 B. Nieva-Echevarria, M. J. Manzanos, E. Goicoechea and M. D. Guillen, *Compr. Rev. Food Sci. Food Saf.*, 2015, **14**, 67–80.
5 C. Andre, I. Castanheira, J. M. Cruz, P. Paseiro and A. Sanches-Silva, *Trends Food Sci. Technol.*, 2010, **21**, 229–246.
6 J. R. Frost, C. B. Cheong and T. J. Donohoe, *Synthesis*, 2017, **49**, 910–916.
7 J. Y. Xie, J. Q. Liu, Y. H. Zhang, J. J. Li, Z. C. Li and W. C. Huang, *Org. Prep. Proced. Int.*, 2015, **47**, 236–241.
8 H. Amirfirouzkouhi and A. N. Kharat, *Sep. Purif. Technol.*, 2018, **196**, 132–139.
9 S. Li, J. Cao, Y. Dang, X. Feng, Y. Liu, X. Chen and C. Yang, *Ind. Eng. Chem. Res.*, 2019, **58**, 9314–9321.
10 H. Díaz Velázquez, N. Likhanova, N. Aljammal, F. Verpoort and R. Martínez-Palou, *Energy Fuels*, 2020, **34**, 15525–15556.
11 Y. Y. Xin, Y. F. Hu, Y. C. Wang, S. Q. Jiang, M. C. Li, K. B. Chi, S. Zhang, F. Gao, C. X. Ren, S. Zhang and C. L. Ma, *Fuel*, 2022, **326**, 125034.
12 H. N. Peng, X. M. Peng and D. G. Zheng, *Asian J. Chem.*, 2011, **23**, 1833–1837.
13 M. M. Heravi, B. Baghernejad and H. A. Oskooie, *Mol. Diversity*, 2009, **13**, 395–398.
14 P. Gupta and S. Paul, *Catal. Today*, 2014, **236**, 153–170.
15 M. Bayat and D. Gheidari, *Chemistryselect*, 2022, **7**, 774.
16 V. S. Marakatti, S. Marappa and E. M. Gaigneaux, *New J. Chem.*, 2019, **43**, 7733–7742.
17 H. P. Yan, Y. Yang, D. M. Tong, X. Xiang and C. W. Hu, *Catal. Commun.*, 2009, **10**, 1558–1563.
18 S. Sarish, B. M. Devassy and S. B. Halligudi, *J. Mol. Catal. A: Chem.*, 2005, **235**, 44–51.
19 S. M. Kumbar, G. V. Shanbhag, F. Lefebvre and S. B. Halligudi, *J. Mol. Catal. A: Chem.*, 2006, **256**, 324–334.
20 B. M. Devassy, G. V. Shanbhag, F. Lefebvre and S. B. Halligudi, *J. Mol. Catal. A: Chem.*, 2004, **210**, 125–130.
21 J. Gonzalez-Rodriguez, L. Fernandez, Z. Vargas-Osorio, C. Vazquez-Vazquez, Y. Pineiro, J. Rivas, G. Feijoo and M. T. Moreira, *Nanomaterials*, 2021, **11**, 553.
22 A. Samikannu, L. J. Konwar, K. Rajendran, C. C. Lee, A. Shchukarev, P. Virtanen and J.-P. Mikkola, *Appl. Catal., B*, 2020, **272**, 118987.

23 P. Zhang, X. Mao, R. Mi, L. Wang and B. Yang, *Catal. Lett.*, 2021, **151**, 95–106.
24 P. Zhang, P. Liu, M. Fan, P. Jiang and A. Haryono, *Renewable Energy*, 2021, **175**, 244–252.
25 A. M. D. Lima, E. H. Fragal, B. S. Caldas, T. U. Nakamura, A. F. Rubira and R. Silva, *Microporous Mesoporous Mater.*, 2022, **341**, 112097.
26 D. L. Li, K. G. Chai, X. D. Yao, L. Q. Zhou, K. Y. Wu, Z. H. Huang, J. T. Yan, X. Z. Qin, W. Wei and H. B. Ji, *J. Colloid Interface Sci.*, 2021, **583**, 100–112.
27 L. Zhou, L. L. Peng, J. L. Ji, W. T. Ma, J. L. Hu, Y. T. Wu, J. Geng and X. B. Hu, *J. CO2 Util.*, 2022, **58**, 101910.
28 J. X. Peng, D. Iruretagoyena and D. Chadwick, *J. CO2 Util.*, 2018, **24**, 73–80.
29 Z. Y. Zhang, X. X. Zhang, X. Y. Peng, Z. F. Li, H. R. Chen, X. R. Zhang, Y. W. Gong, C. H. Tan and H. Y. Li, *Environ. Sci. Pollut. Res.*, 2022, **29**, 71100–71112.
30 T. W. Chen, W. B. Zhen, Z. M. Yan, H. T. Lin, G. Y. Chen and S. D. Chen, *Chin. J. Struct. Chem.*, 2018, **37**, 2024–2035.
31 V. Chaudhary and S. Sharma, *J. Porous Mater.*, 2016, **24**, 741–749.
32 H. Balcar and J. Cejka, *Catalysts*, 2019, **9**, 743.
33 Z. Zarghami, M. Ramezani and M. Maddahfar, *Mater. Lett.*, 2015, **152**, 21–24.
34 Y. K. Yu, J. F. Miao, J. X. Wang, C. He and J. S. Chen, *Catal. Sci. Technol.*, 2017, **7**, 1590–1601.
35 Y.-C. Lin and J.-H. Lin, *Catal. Commun.*, 2013, **34**, 41–44.
36 J. Ambati, H. Saiyed and S. E. Rankin, *Phys. Chem. Chem. Phys.*, 2012, **14**, 6617–6627.
37 H. Zhang, X. Liu, M. Lu, X. Hu, L. Lu, X. Tian and J. Ji, *Bioresour. Technol.*, 2014, **169**, 800–803.
38 N. B. Karlstedt, M. V. Anokhin and I. P. Beletskaya, *Russ. Chem. Bull.*, 2013, **62**, 2498–2499.
39 D. Zhao, J. Feng, Q. Huo, N. Melosh, G. H. Fredrickson, B. F. Chmelka and G. D. Stucky, *Science*, 1998, **279**, 548–552.
40 S.-C. Qi, Z.-H. Yang, R.-R. Zhu, X.-J. Lu, D.-M. Xue, X.-Q. Liu and L.-B. Sun, *J. Mater. Chem. A*, 2021, **9**, 24510–24516.
41 S.-C. Qi, X.-Y. Liu, R.-R. Zhu, D.-M. Xue, X.-Q. Liu and L.-B. Sun, *Chem. Eng. J.*, 2022, **430**, 132784.